

DMA-aided MU-MISO Systems for Power Splitting SWIPT via Lorentzian-Constrained Holography

Askin Altinoklu, and Leila Musavian

Abstract—This paper presents an optimal power splitting and beamforming design for co-located simultaneous wireless information and power transfer (SWIPT) users in Dynamic Metasurface Antenna (DMA)-aided multiuser multiple-input single-output (MISO) systems. The objective is to minimize transmit power while meeting users’ signal-to-interference-plus-noise ratio (SINR) and energy harvesting (EH) requirements. The problem is solved via an alternating optimization framework based on semidefinite programming (SDP), where metasurface tunability follows Lorentzian-constrained holography (LCH). In contrast to traditional beamforming architectures, DMA-assisted architectures reduce the need for RF chains and phase shifters but require optimization under the Lorentzian constraint limiting the amplitude and phase optimizations. Hence, the proposed method integrates several LCH schemes, including the recently proposed adaptive-radius LCH (ARLCH), and evaluates nonlinear EH models and circuit noise effects. Simulation results show that the proposed design significantly reduces transmit power compared with baseline methods, highlighting the efficiency of ARLCH and optimal power splitting in DMA-assisted SWIPT systems.

Index Terms—SWIPT, Holographic-MIMO, DMA, reconfigurable intelligent surfaces.

I. INTRODUCTION

DMA, a recently emerging class of holographic multiple-input multiple-output (HMIMO) systems, consist of reconfigurable arrays of microstrip- or waveguide-fed metasurface elements whose electromagnetic responses can be dynamically controlled by tuning parameters for changing the resonant state of elements [1]. This tunability enables analog-domain beamforming without the need for external phase shifters or high-power amplifiers that are typically required in traditional hybrid or fully digital architectures [2]. When integrated with digital precoders, DMAs can establish multiuser MIMO links with fewer RF chains, thereby enabling scalable and energy-efficient transceiver architectures [3].

SWIPT is another key technology for next-generation communication systems, allowing the simultaneous delivery of wireless information transfer (WIT) and wireless power transfer (WPT) [4]. Prior research on SWIPT in traditional MIMO architectures has focused on improving end-to-end energy transfer and spectral efficiency in co-located receivers via power-splitting (PS) and time-switching (TS) schemes [5]. On the other hand, for network with separated energy-harvesting

(EH) and information-decoding (ID) users, beamforming-based approaches were employed to allocate dedicated transmission beams [6]. However, the increasing demand for energy and information transfer in future generation systems calls for large-scale and energy-efficient transceiver architectures, where DMAs can play a significant role due to their hardware simplicity and beamforming flexibility. Despite growing interest, there are only a few works considering DMA-assisted SWIPT systems. Existing works have mainly focused on either WPT [7] or WIT based [2], [8] designs, particularly in near-field communications, leveraging the beam-focusing capability of DMA-assisted millimeter-wave links. Recent studies, such as [9] and [10] considered DMA-aided SWIPT for spectral efficiency and harvested power maximization, respectively; however, both addressed separate EH and ID users, achieved through separate beamforming vectors. In contrast, the co-located SWIPT scenario, where each user simultaneously performs EH and ID remains unexplored for DMA-aided architectures, despite being highly relevant to low-power wireless-powered sensor and internet of things networks.

The design of DMA-assisted PS-SWIPT systems is particularly challenging due to the need for joint optimization of DMA weights, digital precoding vectors, and PS factors. Moreover, DMA weights must be optimized under unique characteristics known as Lorentzian constraints, where amplitudes of elements are dependent on their associated phases sinusoidally [1]. Thus, this unique constraint couples the amplitude and phase responses of each DMA element, resulting in a nonconvex problem that cannot be directly solved using conventional beamforming optimization techniques. Several LCH methods such as phase holography (LCPH), unitary-shift holography (LCUSH), and Amplitude only holography (AOH) have been proposed to address this limitation [11], [12]. More recently, ARLCH method was introduced in [12], achieving superior performance by dynamically determining optimal phase points with an adaptive parameter of peak amplitude of Lorentzian-constraint to minimize the discrepancy between ideal and physically feasible weights.

Based on these observations, this paper aims to address the identified challenges through the following key contributions:

- We propose a novel optimization framework for DMA-assisted PS-SWIPT system for multiuser networks, formulating a joint transmit power minimization problem under simultaneous EH and signal-to-interference-plus-noise ratio (SINR) constraints. The highly coupled nonconvex problem is reformulated into a semidefinite programming (SDP) structure, enabling an efficient and

The authors are with the School of Computer Science and Electronic Engineering, University of Essex, Wivenhoe Park, Colchester CO43SQ, United Kingdom (e-mail: askin.altinoklu, leila.musavian@essex.ac.uk). This work was supported by UK Research and Innovation under the UK government’s Horizon Europe funding guarantee through MSCA-DN SCION Project Grant Agreement No.101072375 [Grant Number: EP/X027201/1].

tractable alternating optimization solution.

- To the best of our knowledge, this is the first work that jointly optimizes DMA weights, digital precoders, and PS ratios under Lorentzian constraints for co-located SWIPT, providing new insights into the challenges arising from the Lorentzian amplitude–phase coupling intrinsic to DMA physics. For this purpose, multiple LCH mapping schemes are considered, and the ARLCH approach is integrated into the DMA-SWIPT scenario to dynamically balance amplitude–phase tradeoffs and reduce projection loss in DMA weight realization.
- Unlike prior DMA-SWIPT studies [9] and [10], the proposed framework also accounts for practical nonlinear EH receiver models and illustrates how their parameters critically affect beamforming performance and transmit power levels.
- Simulation results demonstrate that the proposed ARLCH-based approach for optimal PS-SWIPT achieves substantial transmit power reduction compared with benchmark schemes (AOH, LCUSH, and LCPH), while satisfying both EH and SINR requirements.

Notations: Matrices are denoted by \mathbf{W} , with $\text{Tr}(\mathbf{W})$, \mathbf{W}^T , \mathbf{W}^H , and $\text{Vec}(\mathbf{W})$ representing, trace, transpose, Hermitian conjugate, and vectorization. Vectors are \mathbf{w} , with $\|\mathbf{w}\|$, \mathbf{w}^T , and \mathbf{w}^H indicating Euclidean norm, transpose, and Hermitian conjugate. Scalars are w , with $|w|$ as the absolute value. The Kronecker product is denoted by \otimes .

II. SYSTEM MODEL AND PROBLEM FORMULATION

We consider a multiuser MISO downlink SWIPT system comprising a base station (BS) equipped with a DMA-based hybrid architecture integrated with a digital precoder. The network serves K user equipments (UEs), each requiring a target SINR for information decoding and a minimum harvested energy level.

A. Channel and Path-Loss Modeling

In this paper, we consider spherical wavefront model (SWM) with the near-field channel in a line-of-sight (LoS) condition. For obtaining SWM, we consider a uniform planar array (UPA) consisting of N_r and N_c sub-wavelength elements in the vertical and horizontal directions, yielding a total of $N = N_r N_c$ elements. For this model, the radiation pattern of the elements is well-approximated with:

$$G_e(\psi) = \begin{cases} 6 \cos^g(\psi), & 0 \leq \psi \leq \pi/2, \\ 0, & \pi/2 < \psi \leq \pi, \end{cases} \quad (1)$$

where ψ is the angle measured from the array boresight [13]. The path loss for the user positioned at \mathbf{r}_k due to the (i,l) -th element of the UPA ($\mathbf{r}_{i,l}$) can be expressed with:

$$\gamma_k(i,l) = \sqrt{G_e(\psi)} \frac{\lambda}{4\pi \|\mathbf{r}_k - \mathbf{r}_{i,l}\|} e^{-j\beta_0 \|\mathbf{r}_k - \mathbf{r}_{i,l}\|}, \quad (2)$$

where λ , and β_0 are the free-space wavelength and wavenumber, respectively. The entries $\gamma_k(i,l)$ are the elements of the channel vector $\boldsymbol{\gamma}_k \in \mathbb{C}^{N \times 1}$, i.e., $\boldsymbol{\gamma}_k \triangleq [\gamma_k(1,1), \gamma_k(1,2), \dots, \gamma_k(N_r, N_c)]^H$.

B. DMA Architecture

The reference waves traveling within each DMA radiate through the metasurfaces whose weights are externally controlled by dynamically configurable weights based on LCH ($\mathbf{Q} \in \mathbb{C}^{N \times N_r}$) to achieve analog beamforming. Each DMA is connected to the digital precoder via RF chains, and the weights of reference waves of different DMAs are further controlled by the information encoded linear precoding vectors $\mathbf{w}_m \in \mathbb{C}^{N_r \times 1}$ for all $m \in M$, where $M = \min(K, N_r)$. The propagation of reference waves within the DMAs are captured by $\mathbf{H} \in \mathbb{C}^{N \times N}$, which is a diagonal matrix with elements $\mathbf{H}_{(i-1)N_c+l, (i-1)N_c+l} = e^{-d_{i,l}(\alpha_i + j\beta_i)}$, where $d_{i,l}$ is the position of the l -th element along the i -th microstrip, and α_i, β_i are its attenuation and propagation constants [3]. Based on this, the baseband transmitted signal at DMA-aided BS is expressed as

$$\mathbf{x} = \sum_{m=1}^M \mathbf{x}_m = \sum_{m=1}^M \mathbf{H} \mathbf{Q} \mathbf{w}_m s_m, \quad (3)$$

where s_m denotes the transmitted data symbol associated with the m -th precoding vector \mathbf{w}_m , for all $m \in \{1, \dots, M\}$. In (3), the matrix \mathbf{Q} has a block-diagonal structure, where each block represents the amplitude–phase profile of the metasurface along a distinct DMA microstrip, i.e., each row of the UPA, and is given by

$$\mathbf{Q}_{(i-1)N_c+l, n} = \begin{cases} q_{i,l} \in \mathbb{Q}, & i = n, \\ 0, & i \neq n, \end{cases} \quad (4)$$

where \mathbb{Q} denotes the Lorentzian-profile set characterizing the tunable metasurface elements. Each coefficient $q_{i,l}$ is controlled by varying the resonance frequency of its associated element, for example via external varactor diodes, and satisfies

$$\mathbb{Q} = \left\{ q = \frac{j + e^{j\Phi}}{2} : \Phi \in [0, 2\pi] \right\}. \quad (5)$$

C. SWIPT Signal Modeling

In the considered PS-SWIPT scenario, the received RF signal at UE $_k$ is split by a power splitter into two parts: a fraction ρ_k ($0 < \rho_k < 1$) directed to the information decoder (ID) and the remaining $1 - \rho_k$ directed to the energy harvester (EH). Accordingly, the signal at the ID is given by

$$y_k^{(\text{ID})} = \sqrt{\rho_k} \left(\boldsymbol{\gamma}_k^H \sum_{m=1}^M \mathbf{H} \mathbf{Q} \mathbf{w}_m s_m + n_{a,k} \right) + n_{c,k}, \quad (6)$$

where $n_{a,k} \sim \mathcal{CN}(0, \sigma_{a,k}^2)$, and $n_{c,k} \sim \mathcal{CN}(0, \sigma_{c,k}^2)$ represent the antenna noise at UE $_k$, and the additional noise introduced by baseband conversion in the ID of UE $_k$, respectively. Using (6), the SINR at UE $_k$ is given by

$$\text{SINR}_k = \frac{|\boldsymbol{\gamma}_k^H \mathbf{H} \mathbf{Q} \mathbf{w}_k|^2}{\sum_{\substack{m=1 \\ m \neq k}}^M |\boldsymbol{\gamma}_k^H \mathbf{H} \mathbf{Q} \mathbf{w}_m|^2 + \sigma_k^2}, \quad (7)$$

where $\sigma_k^2 = \sigma_{a,k}^2 + \sigma_{c,k}^2/\rho_k$. Similarly, for the EH part, the received signal at UE_k is expressed by

$$y_k^{(\text{EH})} = \sqrt{1 - \rho_k} \left(\gamma_k^H \sum_{m=1}^M \mathbf{H}\mathbf{Q}\mathbf{w}_m s_m + n_{a,k} \right), \quad (8)$$

while the received power for the EH part is obtained with

$$P_k^{(\text{EH})} = (1 - \rho_k) \sum_{m=1}^M |\gamma_k^H \mathbf{H}\mathbf{Q}\mathbf{w}_m|^2. \quad (9)$$

Then, under the linear EH model, the harvested energy at UE_k is linearly proportional to the received RF power, i.e., $E_k = \eta P_k^{(\text{EH})}$, where $0 < \eta \leq 1$ denotes the energy-harvesting efficiency. For a better representation, the harvested energy can alternatively be described by a logistic nonlinear model [14]:

$$E_k = \frac{\frac{E^{\text{sat}}}{1 + e^{-a(P_k^{(\text{EH})} - b)}} - \frac{E^{\text{sat}}}{1 + e^{ab}}}{1 - \frac{1}{1 + e^{ab}}}, \quad (10)$$

where E^{sat} is the maximum harvestable power before saturation and a and b are circuit-specific logistic parameters.

III. PROBLEM FORMULATION AND SOLUTION

A. Optimization Problem Formulation

In this paper, we consider a PS-SWIPT system under guaranteed QoS requirements for both ID and EH. The objective is to minimize the total transmit power at the DMA-aided BS by jointly designing the precoding vectors \mathbf{w}_k , the DMA weight matrix \mathbf{Q} , and the PS ratios ρ_k . The resulting optimization problem is formulated as

$$\underset{\{\mathbf{w}_k\}_{k=1}^K, \{\rho_k\}_{k=1}^K, \mathbf{Q}}{\text{minimize}} \quad \sum_{k=1}^K \|\mathbf{H}\mathbf{Q}\mathbf{w}_k\|^2 \quad (11a)$$

$$\text{s. t.} \quad \text{SINR}_k(\{\mathbf{w}_k\}, \mathbf{Q}, \rho_k) \geq \delta_k, \quad \forall k, \quad (11b)$$

$$E_k(\{\mathbf{w}_k\}, \mathbf{Q}, \rho_k) \geq E_k^{\text{th}}, \quad \forall k, \quad (11c)$$

$$0 < \rho_k < 1, \quad \forall k, \quad (11d)$$

$$\mathbf{Q} \in \mathbb{Q}^{N \times N_t}, \quad (11e)$$

where δ_k , and E_k^{th} are the SINR and EH thresholds of UE_k, respectively. Constraint (11c) can be equivalently expressed using the received RF power from (9) for both the linear and nonlinear energy-harvesting models as

$$P_k^{(\text{EH})} \geq P_k^{\text{th}}, \quad (12)$$

where

$$P_k^{\text{th}} = \begin{cases} \frac{E_k^{\text{th}}}{\eta}, & \text{(Linear model),} \\ b - \frac{1}{a} \ln \frac{e^{ab}(E^{\text{sat}} - E_k^{\text{th}})}{e^{ab}E_k^{\text{th}} + E^{\text{sat}}}, & \text{(Nonlinear model).} \end{cases}$$

Moreover, the constraint (11b) can be written as:

$$|\gamma_k^H \mathbf{H}\mathbf{Q}\mathbf{w}_k|^2 - \delta_k \sum_{\substack{j=1 \\ j \neq k}}^K |\gamma_k^H \mathbf{H}\mathbf{Q}\mathbf{w}_j|^2 \geq \delta_k (\sigma_{a,k}^2 + \frac{\sigma_{c,k}^2}{\rho_k}). \quad (13)$$

The optimization problem in (11) involves coupled variables, namely the precoding vectors \mathbf{w}_k , the DMA weight matrix \mathbf{Q} , and the PS ratios ρ_k . It involves quadratic terms that appear in a non-convex form, particularly in the coupling of \mathbf{Q} and \mathbf{w}_k . Furthermore, the Lorentzian constraint in (11e) is also non-convex, since the amplitude and phase of each DMA element are intrinsically linked through the sinusoidal relationship described in (5). As a result, solving this problem is challenging; in the next section, we present a tractable solution approach.

B. Optimizing the Digital Precoder and PS Ratio

When the DMA weight matrix \mathbf{Q} and the PS ratios ρ_k are fixed, the problem in (11) can be reformulated as the following SDP:

$$\begin{aligned} & \underset{\{\mathbf{w}_k, \rho_k\}}{\text{min}} \quad \sum_{k=1}^K \text{Tr}(\mathbf{Z}\mathbf{W}_k) \\ \text{s. t.} \quad & \frac{1}{\delta_k} \text{Tr}(\mathbf{P}_k \mathbf{W}_k) - \sum_{\substack{m=1 \\ m \neq k}}^K \text{Tr}(\mathbf{P}_k \mathbf{W}_m) \geq \sigma_a^2 + \frac{\sigma_c^2}{\rho_k}, \quad \forall k, \\ & \sum_{m=1}^K \text{Tr}(\mathbf{P}_k \mathbf{W}_m) \geq \frac{P_k^{\text{th}}}{1 - \rho_k}, \quad \forall k, \\ & \text{rank}(\mathbf{W}_k) = 1, \quad \forall k, \\ & 0 < \rho_k < 1, \quad \forall k, \\ & \mathbf{W}_k \succeq 0, \quad \forall k, \end{aligned} \quad (14)$$

where $\mathbf{Z} = (\mathbf{H}\mathbf{Q})^H \mathbf{H}\mathbf{Q}$, $\mathbf{P}_k = (\gamma_k^H \mathbf{H}\mathbf{Q})^H \gamma_k^H \mathbf{H}\mathbf{Q}$, and $\mathbf{W}_k = \mathbf{w}_k \mathbf{w}_k^H$. Since the objective function and all constraints except the rank-one condition are affine in \mathbf{W}_k , the relaxed problem, obtained by dropping $\text{rank}(\mathbf{W}_k) = 1$, is convex and can be efficiently solved using convex-optimization tools such as CVX [15]. Moreover, it can be shown that this relaxed SDP provides rank-one optimal solutions [16]. Consequently, the digital precoding vectors \mathbf{w}_k ($\forall k$) can be obtained directly from the principal eigenvectors of the corresponding optimal matrices \mathbf{W}_k , ensuring optimality for the given \mathbf{Q} and ρ_k .

C. Optimizing the DMA Weights

Optimizing (11) for DMA weights \mathbf{Q} is challenging due to non-convex Lorentzian-constraint introduced with (11e). Hence, for the solution of this problem, we introduce in here two-tier optimization problem, i.e., first for the given \mathbf{w}_k and ρ_k , the problem was reformulated in the SDP form for the relaxed condition of Lorentzian-constraint (11e) (Lorentzian-relaxed), then the projection based scheme for obtaining Lorentzian-constrained weights from the solution of unconstrained problem (unconstrained in terms of (11e)) is used to obtain final solution of \mathbf{Q} .

1) *SDP Formulation:* When the precoding vectors \mathbf{w}_k and the PS ratios ρ_k are fixed for $\forall k$, the Lorentzian-relaxed form of (11) for optimizing DMA weights can be formulated in SDP form to make it tractable against variable \mathbf{Q} . Starting from

the transmitted and received signals, we reformulate them as functions of \mathbf{Q} via linear-algebra manipulations [8]:

$$\begin{aligned} \mathbf{x}_m &= (\mathbf{w}_m^T \otimes \mathbf{H}) \text{vec}(\mathbf{Q}), \\ y_{k,m} &= (\mathbf{w}_m^T \otimes (\gamma_k^H \mathbf{H})) \text{vec}(\mathbf{Q}). \end{aligned}$$

Based on these expressions, the optimization problem for determining \mathbf{Q} can be written in a rank-1 relaxed SDP form:

$$\begin{aligned} & \underset{\tilde{\mathbf{Q}}}{\text{minimize}} && \sum_{m=1}^M \text{Tr}(\tilde{\mathbf{B}}_m \tilde{\mathbf{Q}}) \\ \text{s.t.} &&& \text{Tr}(\tilde{\mathbf{C}}_{k,k} \tilde{\mathbf{Q}}) - \delta_k \sum_{\substack{m=1 \\ m \neq k}}^M \text{Tr}(\tilde{\mathbf{C}}_{k,m} \tilde{\mathbf{Q}}) - \delta_k \sigma_k^2 \geq 0, \quad \forall k, \\ &&& \sum_{m=1}^M \text{Tr}(\tilde{\mathbf{C}}_{k,m} \tilde{\mathbf{Q}}) \geq \frac{P_k^{\text{th}}}{1 - \rho_k}, \quad \forall k, \\ &&& \tilde{\mathbf{Q}} \succeq 0. \end{aligned} \tag{15}$$

where $\tilde{\mathbf{B}}_m = (\mathbf{w}_m^T \otimes \mathbf{H})^H (\mathbf{w}_m^T \otimes \mathbf{H})$, $\tilde{\mathbf{C}}_{k,m} = (\mathbf{w}_m^T \otimes (\gamma_k^H \mathbf{H}))^H (\mathbf{w}_m^T \otimes (\gamma_k^H \mathbf{H}))$, and $\tilde{\mathbf{Q}} = \tilde{\mathbf{q}} \tilde{\mathbf{q}}^H$. In $\tilde{\mathbf{Q}}$, $\tilde{\mathbf{q}} \in \mathbb{C}^{N \times 1}$ denotes the reduced vector obtained from $\mathbf{q} = \text{vec}(\mathbf{Q}) \in \mathbb{C}^{L \times 1}$, where $L = N_r^2 N_c$, by removing all zero entries. Accordingly, the rows and columns of $\tilde{\mathbf{C}}_{k,m}$ and $\tilde{\mathbf{B}}_m$ are formed by deleting the components corresponding to those zero entries. In (15), the objective function is convex and all constraints are affine in $\tilde{\mathbf{Q}}$, so (15) defines a convex optimization problem that can be efficiently solved using CVX [15]. Its solution gives the matrix $\tilde{\mathbf{Q}}^* \in \mathbb{C}^{N \times N}$, if the condition is valid for $\text{rank}(\tilde{\mathbf{Q}}^*) = 1$, the unconstrained DMA weights can be recovered from the dominant eigenvector of $\tilde{\mathbf{Q}}^*$ since $\tilde{\mathbf{Q}}^* = \tilde{\mathbf{q}}^* \tilde{\mathbf{q}}^{*H}$, otherwise best rank-1 approximation can be used to obtain solution for DMA weights [12].

2) *Lorentzian Mapping*: Once the solution for the unrestricted DMA weights $\tilde{\mathbf{q}}^*$ is obtained by solving the SDR problem in (15), it must be projected onto the Lorentzian circle defined in (5). This projection can be expressed through the mapping operator

$$\mathbf{q}^{\text{LCH}} = \mathcal{M}(\tilde{\mathbf{q}}^*; \Omega), \tag{16}$$

where $\mathbf{q}^{\text{LCH}} \in \mathbb{Q}^{N \times 1}$ and Ω denotes the chosen Lorentzian-constrained mapping scheme. For this operator, the recently proposed mapping method, namely the Adaptive-Radius Lorentzian-Constrained Holography (ARLCH), is integrated into the proposed beamforming algorithm for optimizing DMA weights [12]. In ARLCH, the diameter of the Lorentzian circle is relaxed while determining the optimal phase points of the Lorentzian-constrained DMA weights from the unconstrained solution. The projection is performed at an adaptively optimal diameter (Lemma 1, [12]) that minimizes the discrepancy between the ideal unconstrained weights and the feasible Lorentzian-constrained weights. Then, these optimal phase points are used to determine Lorentzian-constrained weights using unitary Lorentzian-circle (5). Overall, ARLCH¹ enables

¹For further details and derivations, the reader is referred to [12].

dynamic phase optimization on a relaxed Lorentzian circle with an adaptive radius, thereby providing additional degrees of freedom to control the sinusoidal variations imposed by Lorentzian constraints. In contrast, traditional Lorentzian projection schemes map the solution onto a unitary Lorentzian circle, which limits the flexibility of controlling amplitude variations of the DMA weights. As baseline methods to ARLCH, we consider the following classical LCH schemes as a mapping operator $\mathcal{M}(\cdot; \Omega)$: LCPH, LCUSH, and AOH, described below.

Given the SDR solution of (15) for tier-1 DMA weight optimization,

$$q_n^* = |q_n^*| e^{j\psi_n^*}, \quad \forall n \in \{1, \dots, N\},$$

the Lorentzian-constrained DMA weights for traditional schemes are obtained by using phases of SDR solution $\hat{q}_n^* = e^{j\psi_n^*}$ as follows:

- **LCPH**:

$$q_n^{\text{LCH}} = \begin{cases} \sin(\psi_n^*) e^{j\psi_n^*}, & 0 \leq \psi_n^* \leq \pi, \\ 0, & \pi < \psi_n^* \leq 2\pi, \end{cases}$$

which preserves the SDR phases while imposing Lorentzian amplitude shaping.

- **LCUSH**:

$$q_n^{\text{LCH}} = \frac{1}{2}(j + e^{j\psi_n^*}),$$

which simply adds the j term to the SDR phase-aligned solution.

- **AOH**:

$$q_n^{\text{LCH}} = \sin(\theta_n) e^{j\theta_n}, \quad \theta_n = \arcsin\left(\frac{1 + \cos(\psi_n^*)}{2}\right),$$

which maps DMA weights based on amplitude-optimized holography projections.

Following the above derivations, the solution procedure for Problem (11) is summarized in Algorithm 1, which alternately updates the DMA weights and the precoder and PS variables. The alternating optimization under the selected mapping scheme Ω yields the optimal DMA-assisted PS-SWIPT solution, where the proposed method adopts ARLCH

Algorithm 1 Proposed Algorithm for Solving Problem (11)

- 1: Initialize DMA weights $\mathbf{Q}^{(0)}$ randomly
 - 2: **[Start]** Solve SDR (14) for $\{\mathbf{w}_k^{(0)}\}, \{\rho_k^{(0)}\}$ given $\mathbf{Q}^{(0)}$
 - 3: **for** $t = 1$ to T_{\max} **do**
 - 4: **Step 1: DMA Weight Update:** Solve SDR (15) for unconstrained $\tilde{\mathbf{q}}^{*(t)}$
 - 5: Lorentzian projection: $\mathbf{q}^{(t)} = \mathcal{M}(\tilde{\mathbf{q}}^{*(t)}; \Omega)$
 - 6: **Step 2: Precoder and Splitting Update:** Solve SDR (14) for $\{\mathbf{w}_k^{(t)}\}$ and $\{\rho_k^{(t)}\}$ given updated $\mathbf{Q}^{(t)}$
 - 7: Update transmit power $P_{\text{Tx}}^{(t)}$
 - 8: **Convergence Check:** If $P_{\text{Tx}}^{(t)} \leq P_{\text{Tx}}^{(t-1)}$, update $P_{\text{Tx}}^{(f)}$, $\{\mathbf{w}_k^{(f)}\}, \{\rho_k^{(*)}\}, \mathbf{Q}^*$
 - 9: **end for**
 - 10: **Output:** Optimized $\mathbf{Q}^{(f)}$, $\{\mathbf{w}_k^{(f)}\}$, and $\{\rho_k^{(f)}\} \forall k \in K$
-

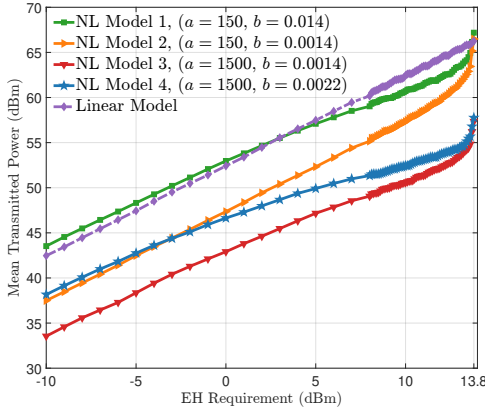


Fig. 1. Transmitted power versus EH power requirement (E_k^{th}) for different energy harvesting models with $K = 2$ and $\delta_k = 10\text{dB}$.

for this operator. Executing Algorithm 1 without the mapping step provides the unrestricted weight solution of DMA (DMA-UW), serving as an upper performance bound by disregarding phase limitations imposed Lorentzian-constraint (5). The overall computational complexity is dominated by the SDP solvers in CVX, with order $\mathcal{O}(\max K, N^4 N^{1/2} \log(1/\epsilon))$ [17], which is polynomial in both the total number of elements N and number of users K .

IV. NUMERICAL RESULTS

In the numerical results, the DMA array is assumed to be on the xy -plane, while the UEs are located within the near-field region in the xz -plane, defined by the radius range $0.1d_F < r < 1d_F$. Here, d_F denotes the Fraunhofer distance, given by $d_F = \frac{2D^2}{\lambda}$ where D and λ represent the antenna aperture length and wavelength, respectively. The carrier frequency is set to $f = 28$ GHz. The DMA parameters are selected for attenuation constant $\alpha = 0.6 \text{ m}^{-1}$ and phase constant $\beta = 827.67 \text{ rad/m}$, with inter-element spacing of $\lambda/2$ along both x - and y -directions. The DMA configuration consists of $N_r = 8$ RF chains and $N_e = 64$ metasurface elements per RF chain, resulting in an effective aperture of $D \approx 0.33 \text{ m}$ and a corresponding Fraunhofer distance of $d_F \approx 21.5 \text{ m}$. The antenna noise power is set to $\sigma_a^2 = -70 \text{ dBm}$ in all simulations.

As an initial analysis, we evaluate the performance of the proposed approach, combining ARLCH-based DMA mapping with optimal PS, under different NL energy harvesting models defined in (10), along with a linear EH reference. Four NL models are considered with parameters adopted from the literature [14], all exhibiting a saturation power of $E^{\text{sat}} = 13.8 \text{ dBm}$. The linear model assumes a constant conversion efficiency of $\eta = 0.5$. The analysis is performed for a two-user scenario ($K = 2$), where both users are aligned in the same direction with UE₁ located at $(0, 0, 0.1d_F)$ and UE₂ at $(0, 0, 0.3d_F)$. In this setup, beamforming is achieved through near-field beam focusing based on the spherical-wave model. The results in Fig. 1 depict the transmitted power versus the EH power requirement E_k^{th} for a guaranteed SINR of

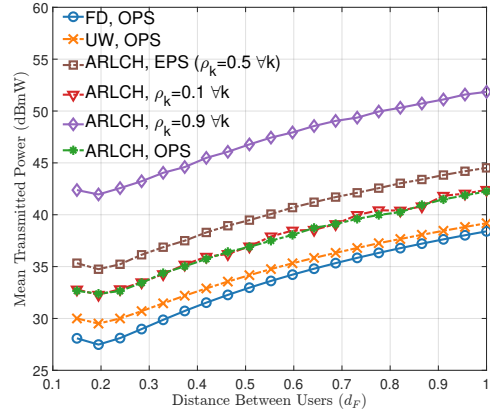


Fig. 2. Transmitted power vs. user separation distance for $K = 2$, $\delta_k = 10 \text{ dB}$, $E_k^{\text{th}} = -10 \text{ dBmW}$, and $\sigma_c = -50 \text{ dB}$.

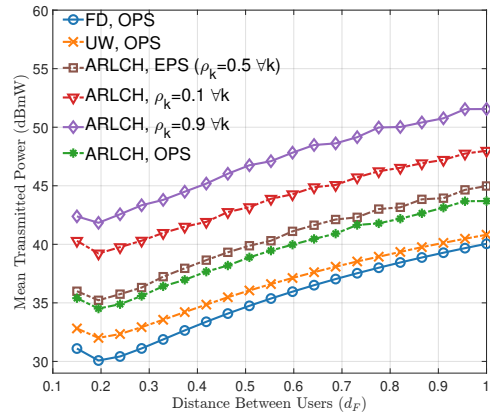


Fig. 3. Transmitted power vs. user separation distance for $K = 2$, $\delta_k = 10 \text{ dB}$, $E_k^{\text{th}} = -10 \text{ dBmW}$, and $\sigma_c = -30 \text{ dBm}$.

$\delta_k = 10 \text{ dB}$. As expected, the linear model shows a monotonic increase in transmitted power with E_k^{th} , whereas the NL models exhibit saturation behavior near E^{sat} . Among the NL models, higher charging rate a values lead to lower transmitted power, while a smaller sensitivity parameter b further reduces the required transmit power for the same a . The results demonstrate the robustness of the proposed beamforming approach in accurately capturing the nonlinear EH behavior with changing parameters, highlighting the importance of precise nonlinear modeling for reliable performance prediction. We next examine the effect of PS and baseband conversion noise on the proposed ARLCH-based DMA beamforming with optimal PS (OPS). A two-user scenario ($K = 2$) is considered, where UE₁ is fixed at $(0, 0, 0.1d_F)$ and UE₂ is swept along the z -axis as $(0, 0, \zeta d_F)$, with $\delta_k = 10 \text{ dB}$ and $E_k^{\text{th}} = -10 \text{ dBmW}$. As baselines, we include the FD case (64×8 array with 512 RF chains) and the DMA-UW. Equal power splitting (EPS) and fixed splitting ($\rho_k = 0.1, 0.9$) are compared with OPS under $\sigma_c = -50$ and -30 dBm in Fig. 2, and Fig. 3, respectively. The results show that as UE₂ moves farther from the DMA, the transmitted power increases in all cases, since satisfying the EH requirement becomes more challenging at larger distances.

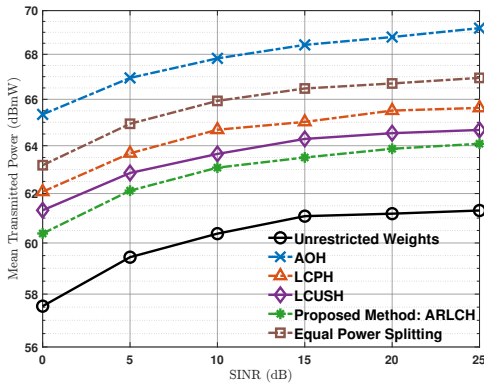


Fig. 4. Mean transmitted power vs. SINR for Monte Carlo realizations under different LCH schemes with $E_k^{\text{th}} = -10$ dBmW and $K = 4$.

When UE₂ moves closer than $(0, 0, 0.2d_F)$, increased inter-user interference raises the required transmit power, despite ease of EH requirement guarantee with a lower path-loss. At lower conversion noise ($\sigma_c = -50$ dB), where the SINR constraint is easier to meet, the OPS performance converges toward $\rho_k = 0.1$ performance, indicating WPT dominance, as shown in Fig. 2. Conversely, at high noise (-30 dB) it shifts toward EPS with balanced WIT–WPT tradeoff as depicted in Fig. 3. These results confirm the effectiveness of the proposed OPS-based beamforming for adaptive power allocation under varying channel and hardware conditions. Finally, comparison with DMA-UW and FD architectures illustrates the impact of the Lorentzian constraint: while amplitude–phase coupling in LCH significantly limits performance, the small performance gap between DMA-UW and FD validates the robustness of the proposed SDP-based optimization framework.

To examine further the impact of different LCH schemes, Monte Carlo simulations with 200 realizations are conducted for AOH, LCPH, LCUSH, and DMA-UW, alongside the proposed ARLCH approach and its EPS variant. Fig. 4 illustrates the mean transmitted power versus SINR threshold δ_k . Results indicate that AOH performs poorly due to its amplitude-only optimization, failing to achieve proper phase alignment, while LCPH also degrades performance since significant number of the DMA elements are deactivated to preserve phase matching. LCUSH improves performance slightly by activating more elements, yet the proposed ARLCH achieves the best performance by adaptively balancing amplitude-phase relations, reducing grating lobes, and lowering transmit power while maintaining SINR targets. Conversely, EPS under ARLCH significantly degrades performance, emphasizing the importance of optimal power splitting in PS-SWIPT systems. These results clearly demonstrate the robustness of proposed approach and also highlight the significance of selection of proper LCH scheme.

V. CONCLUSION

This paper presented an SDR-based framework for optimal PS-SWIPT in DMA-assisted multiuser MISO systems. A joint optimization of DMA weights, precoding, and PS ratios was

achieved through an alternating optimization algorithm with Lorentzian-mapping scheme based on ARLCH. The results confirm the critical role of mapping schemes, which are unique to DMA architectures, in conjunction with optimal PS for effectively balancing the EH–ID trade-off. The results demonstrated that the proposed approach effectively captures nonlinear EH characteristics, minimizes transmit power, and outperforms conventional LCH. Future work can explore its extension to non-line of sight scenario with electromagnetic compliant modeling of DMA.

REFERENCES

- [1] D. R. Smith, O. Yurduseven, L. P. Mancera, P. Bowen, and N. B. Kundtz, "Analysis of a waveguide-fed metasurface antenna," *Phys. Rev. Appl.*, vol. 8, p. 054048, Nov 2017.
- [2] H. Zhang, N. Shlezinger, F. Guidi, D. Dardari, M. F. Imani, and Y. C. Eldar, "Beam focusing for near-field multiuser MIMO communications," *IEEE Trans. Commun.*, vol. 21, no. 9, pp. 7476–7490, 2022.
- [3] N. Shlezinger, O. Dicker, Y. C. Eldar, I. Yoo, M. F. Imani, and D. R. Smith, "Dynamic metasurface antennas for uplink massive MIMO systems," *IEEE Trans. Commun.*, vol. 67, no. 10, pp. 6829–6843, 2019.
- [4] C. Psomas, K. Ntougias, N. Shanin, D. Xu, K. Mayer, N. M. Tran, L. Cottatellucci, K. W. Choi, D. I. Kim, R. Schober, and I. Krikidis, "Wireless information and energy transfer in the era of 6G communications," *Proc. IEEE*, vol. 112, no. 7, pp. 764–804, 2024.
- [5] R. Zhang and C. K. Ho, "MIMO broadcasting for simultaneous wireless information and power transfer," *IEEE Trans. Wireless Commun.*, vol. 12, no. 5, pp. 1989–2001, 2013.
- [6] J. Xu, L. Liu, and R. Zhang, "Multiuser MISO beamforming for simultaneous wireless information and power transfer," *IEEE Trans. Signal Process.*, vol. 62, no. 18, pp. 4798–4810, 2014.
- [7] H. Zhang, N. Shlezinger, F. Guidi, A. Guerra, D. Dardari, M. F. Imani, and Y. C. Eldar, "Near-field beam focusing for wireless power transfer with dynamic metasurface antennas," *IEEE Internet Things J.*, vol. 12, no. 12, pp. 18 596–18 605, 2025.
- [8] A. Altinoklu and L. Musavian, "Investigation of holographic beamforming via dynamic metasurface antennas in QoS guaranteed power efficient networks," in *2025 Joint EuCNC and 6G Summit*, 2025, pp. 542–547.
- [9] K. Huang, L. You, M. Qian, and X. Gao, "MetaSWIPT: DMA-assisted multi-user MISO downlink simultaneous wireless information and power transfer," *IEEE Wireless Commun. Lett.*, vol. 13, no. 4, pp. 1048–1052, 2024.
- [10] K. Huang, L. You, M. Qian, B. Jiang, and X. Gao, "QoS-guaranteed mimo SWIPT assisted by dynamic metasurface antenna," *IEEE Trans. Veh. Technol.*, pp. 1–6, 2025.
- [11] P. T. Bowen, M. Boyarsky, L. M. Pulido-Mancera, D. R. Smith, O. Yurduseven, and M. Sazegar, "Optimizing polarizability distributions for metasurface apertures with Lorentzian-constrained radiators," *arXiv preprint arXiv:2205.02747*, 2022.
- [12] A. Altinoklu and L. Musavian, "Lorentzian-constrained holographic beamforming optimization in multi-user networks with dynamic metasurface antennas," 2025. [Online]. Available: <https://arxiv.org/abs/2505.08356>
- [13] S. W. Ellingson, "Path loss in reconfigurable intelligent surface-enabled channels," in *Proc. IEEE 32nd Annu. Int. Symp. Pers., Indoor Mobile Radio Commun. (PIMRC)*, Helsinki, Finland, Sep 2021, pp. 829–835.
- [14] E. Boshkovska, D. Ng, N. Zlatanov, and R. Schober, "Practical nonlinear energy harvesting model and resource allocation for SWIPT systems," *IEEE Commun. Lett.*, vol. 19, no. 12, pp. 2082–2085, 2015.
- [15] M. Grant and S. Boyd, "CVX: Matlab software for disciplined convex programming, version 2.1," <https://cvxr.com/cvx>, 2014.
- [16] M. Bengtsson and B. Ottersten, "Optimal and suboptimal transmit beamforming," in *Handbook of Antennas in Wireless Communications*, L. C. Godara, Ed. Boca Raton, FL: CRC Press, 2001.
- [17] Z.-q. Luo, W.-k. Ma, A. M.-c. So, Y. Ye, and S. Zhang, "Semidefinite relaxation of quadratic optimization problems," *IEEE Signal Process. Mag.*, vol. 27, no. 3, pp. 20–34, 2010.